Nonlinear Observer-based Tracking Control of Link Stress and Elevation for a Tethered Aerial Robot using Inertial-only Measurements

Marco Tognon[1,2] and Antonio Franchi[1,2]

Abstract— **This work deals with a comprehensive version of the tethered aerial vehicle problem including all the three possible link cases: cable, strut, and bar. We prove the dynamic feedback linearizability and differential flatness of the system with respect to the elevation of the vehicle and the stress applied to the link. Moreover we prove the observability of the system using only on-board inertial sensors (i.e., only a gyroscope plus an accelerometer). We design a globally convergent nonlinear controller based on the concurrent use of a dynamic feedback linearization control and a state estimator based on a nonlinear state/output transformation and a high gain observer scheme. The controller/observer algorithm is thus able to globally control elevation and stress (both tension and compression) along independent time-varying trajectories only resorting to inertial measurements. The stability of the controlled system is theoretically proven and its behavior is shown by means of extensive dynamical simulations.**

I. INTRODUCTION

Aerial robotics is nowadays the focus of many researches in the robotics field, with an enormous increasing interest over the last decade. The recently technological advances, made aerial robots (also referred to as aerial vehicles, UAVs, or UASs in the literature) extremely versatile and usable in many applications, ranging, e.g., from aerial monitoring to search and rescue. Although they were mainly used as remote and moving sensors, nowadays, their use for physically interactive tasks has become a very popular topic.

In addition to the cooperative transportation case [1], cables are exploited also in systems where one vehicle is tethered to a ground station. In this case the cable can be used to provide energy and a high-bandwidth communication channel. These systems could find direct application for tasks such as surveillance, border protection, temporary communication relay and so on [2], [3]. The tethered flight solution could be exploited also to improve the hover stability in the presence of wind or during dangerous maneuvers, e.g., landing and take off from a moving platform as a ship in the presence of rough sea (see [4] and references therein).

A controller is presented in [5] to stabilize the elevation of a cable-tethered aerial vehicle to a constant value using only inertial onboard sensors. The proposed method is tested on a real quadrotor and relies on a quasi-static assumption. A different controller is presented in [6] which is also able to ensure the positivity of the cable tension.

In this work we solve a generalization of the problems considered in [5], [6]. First of all, we consider the possibility of having a more generic link, either a cable, a strut, or a bar. Second of all we consider a tracking problem for time-varying desired elevation trajectories, instead of just a regulation to a constant desired elevation. Finally, we also consider the problem of simultaneously letting the link stress track *any time-varying force trajectory* that can assume values both in the positive (tensions) and negative (compressions) domains, instead of only ensuring the positivity of the stress [6]. In this way, for example, our control method can be used to follow a certain elevation trajectory while precisely regulating the stress of the link on the basis of its mechanical strength thus avoiding breakages due to excessive tensions or compressions.

The first main contribution of the paper is the design of a nonlinear controller based on dynamic feedback linearization. The second one is the design of a nonlinear observer which uses inertial sensors only. Observation works in dynamics conditions, not only in the quasi-static case [5]. The stability of the controlled/observed system is both theoretically proven and validated through extensive simulations.

Finally, another important contribution of this paper is the thorough investigation of the intrinsic properties of the system, such as exact linearizability with dynamic feedback, flatness, state observability, and trajectory feasibility.

The paper is organized as follows. In Sec. II we derive the dynamic model of the system and the explicit characterization of the internal stress of the link. Then, in Sec. III we show dynamic feedback linearizability of the system with respect to elevation and stress of the link and the related nonlinear controller, moreover we ascertain the flatness property of the system. In Sec. IV we develop a nonlinear observer of the state based on onboard inertial-only measurements. Simulation results are presented in Sec. V. Conclusions and future developments are shown in Sec. VI.

II. DYNAMIC MODEL

Similarly to the original problem defined in [5], [6] we consider a system composed by an underactuated flying vehicle lying on a vertical plane that is connected to the ground through a *link*, as depicted in Fig. 1[1]. Like [5], [6] we assume that the link has a negligible mass and inertia, it is not deformable, and its elasticity is minor in the operative conditions. Therefore, the link has a fixed length $l \in \mathbb{R}_{>0}$.

We denote with $\varphi \in \mathbb{R}$ the *elevation* of the link, i.e., the angle that it forms with the horizon. With $f_L \in \mathbb{R}$ we denote

---

[1]CNRS, LAAS, 7 Avenue du Colonel Roche, F-31400 Toulouse, France. `mtognon@laas.fr`, `antonio.franchi@laas.fr`

[2]Univ de Toulouse, LAAS, F-31400 Toulouse, France

[1]Consideration of the 2D model has been done often in the related literature and does not limit the range of the results. In fact, the 2D case captures most of the nonlinear and challenging features of the problem.
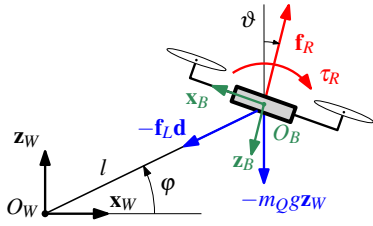
Fig. 1: Representation of the system and its mainly variables.

the *link stress*, i.e., the internal force that is exerted on the link along its longitudinal line. If $f_L > 0$ then the link is pulled and the stress is a *tension*, viceversa, if $f_L < 0$ then the link is compressed and the stress is called a *compression*.

We depart from [5], [6] by adding three more 'challenges' to the original problem. First of all, we consider the simultaneous control of f_L and φ instead of only controlling φ. Second of all, we consider here a tracking problem for the controlled quantities, i.e., their servoing to a time-varying trajectory, instead of regulation to a constant value.[2] Finally, we consider the more general case of a link that can be either a cable, a strut, or a bar (instead of the cable-only case considered in the original problem). We recall that cables, struts, and bars are structural element designed to resist only to tension, compression, and generic stress, respectively.

The two ends of the link are attached to the vehicle center of mass (CoM) and to a *fixed point*, respectively. Connection is made in such a way that no rotational constraint holds on the two ends. Finally, the aerial vehicle is modeled as a rigid body, and we denote with $m_R \in \mathbb{R}_{>0}$ and $J_R \in \mathbb{R}_{>0}$ the mass and the rotational inertia of the vehicle, respectively.

Although we consider here a 2D problem it is still convenient to define our frames in 3D, in order, e.g., to have a properly defined angular velocity vector for the aerial vehicle. Consider in particular two frames: a *world frame*, $\mathscr{F}_W$, with unit vectors along the axes denoted by $\{\mathbf{x}_W, \mathbf{y}_W, \mathbf{z}_W\}$ and origin O_W set on the fixed point, and a *body frame*, $\mathscr{F}_B$, which is rigidly attached to the vehicle, with unit vectors denoted by $\{\mathbf{x}_B, \mathbf{y}_B, \mathbf{z}_B\}$ and origin O_B set on the vehicle CoM, described on $\mathscr{F}_W$ by $\mathbf{p}_B = [x_B\ y_B\ z_B]^T$, where $y_B = 0$. The axes $\mathbf{y}_W$ and $\mathbf{y}_B$ are parallel to each other and both perpendicular to the vertical plane where the system evolves, see Fig. 1. The vehicle motion on the $\{\mathbf{x}_W, \mathbf{z}_W\}$ plane can be controlled acting on two inputs: the intensity $f_R \in \mathbb{R}$ of the thrust force $\mathbf{f}_R = -f_R \mathbf{z}_B \in \mathbb{R}^3$; and the torque $\tau_R \in \mathbb{R}$ acting about the $\mathbf{y}_B$ axis.

Since the motion of the vehicle CoM is constrained on a circle of radius l, the system is completely described by the generalized coordinates $\mathbf{q} = (\varphi, \vartheta)$, where φ and ϑ are the *elevation* of the link (defined before) and the *attitude* of the vehicle, respectively. Deriving kinematic and potential energy, omitted for the limited space, and applying the Euler-Lagrange equation we obtain the system model:

$$m_R l \ddot{\varphi} = -m_R g \cos\varphi + f_R \cos(\varphi + \vartheta) \tag{1}$$

$$J_R \ddot{\vartheta} = \tau_R. \tag{2}$$

[2]In [6] it is guaranteed only the positivity of the stress, while here we allow exact tracking of any stress trajectory.

Considering the motion system constraint, the acceleration of the CoM of the vehicle, with respect $\mathscr{F}_W$, is

$$\ddot{\mathbf{p}}_B = -l\mathbf{d}\dot{\varphi}^2 + l\mathbf{d}^{\perp}\ddot{\varphi}, \tag{3}$$

where $\mathbf{d} = [\cos\varphi\ 0\ \sin\varphi]^T$ and $\mathbf{d}^{\perp} = [-\sin\varphi\ 0\ \cos\varphi]^T$ are unit vectors, in $\mathbb{R}^3$, parallel and perpendicular to the link, respectively. The balance equation of all the forces is

$$m_R \ddot{\mathbf{p}}_B = -f_L \mathbf{d} - f_R \mathbf{z}_B - m_R g \mathbf{z}_W. \tag{4}$$

The stress f_L can be retrieved by projecting the equation (4) along the link axis

$$f_L = -m_R g \sin\varphi + f_R \sin(\varphi + \vartheta) + m_R l \dot{\varphi}^2. \tag{5}$$

The problem that we are facing in this paper is that of designing a control law for the inputs (f_R, τ_R) that is able to asymptotically steer (φ, f_L) along any smooth desired trajectory (φ^d, f_L^d) making use only of an accelerometer and a gyroscope mounted on-board. Moreover, regardless the proposed solution, we aim at investigating the intrinsic characteristics of the system, as dynamic feedback linearizability, flatness and its observability.

III. DYNAMIC DECOUPLING CONTROL

In order to study the system and design the controller, we define $\mathbf{x} = \begin{bmatrix} \varphi & \dot{\varphi} & \vartheta & \dot{\vartheta} \end{bmatrix}^T = [x_1\ x_2\ x_3\ x_4]^T$ and $\mathbf{u} = [f_R\ \tau_R]^T = [u_1\ u_2]^T$ as the state and input vectors of the system, respectively. Rewriting (1) and (2) in the state-space form we have

$$\dot{x}_1 = x_2 \tag{6a}$$
$$\dot{x}_2 = a_1 \cos x_1 + a_2 \cos(x_1 + x_3) u_1 \tag{6b}$$
$$\dot{x}_3 = x_4 \tag{6c}$$
$$\dot{x}_4 = a_3 u_2, \tag{6d}$$

where the constant model parameters are

$$a_1 = -g/l, \qquad a_2 = 1/(m_R l), \qquad a_3 = 1/J_R.$$

To control the elevation and the stress of the link, we consider as outputs of the system the variables $\mathbf{y} = [\varphi\ f_L]^T = [y_1\ y_2]^T$.

Using a feedback linearization approach, we show now how the nonlinear system can be completely transformed in an equivalent controllable and decoupled linear system. First of all, we differentiate the outputs until the inputs appear. From (5) and (6), the outputs can be written as

$$y_1 = x_1 \tag{7a}$$
$$y_2 = -m_R g \sin x_1 + m_R l x_2^2 + \sin(x_1 + x_3) u_1. \tag{7b}$$

We can see that y_2 already contains the input u_1, while y_1 has to be differentiated twice, obtaining

$$\begin{bmatrix} y_1^{(2)} \\ y_2 \end{bmatrix} = \begin{bmatrix} a_1 \cos x_1 \\ m_R l x_2^2 - m_R g \sin x_1 \end{bmatrix} + \underbrace{\begin{bmatrix} a_2 \cos(x_1 + x_3) & 0 \\ \sin(x_1 + x_3) & 0 \end{bmatrix}}_{\mathbf{E}(\mathbf{x})} \mathbf{u}, \tag{8}$$

where $\bullet^{(n)} = \frac{d^n \bullet}{dt^n}$ indicates the n-th time-derivative, for $n \geq 1$. We can observe that the decoupling matrix $\mathbf{E}(\mathbf{x})$ is always singular which means that the system is not linearizable with a static feedback. In these cases one can delay the appearance of the input u_1 in y_2 (i.e., increasing the relative degree of

y_2) by adding one or more integrators in the input channel u_1 thus resulting in a dynamic compensator. To this aim, we redefine the input as $\bar{\mathbf{u}} = [\ddot{u}_1 \ u_2]^T = [\bar{u}_1 \ \bar{u}_2]^T$, considering the acceleration of the thrust intensity as new controllable input, $\ddot{u}_1 = \ddot{f}_R$. The system is now described by the extended state $\bar{\mathbf{x}} = \begin{bmatrix} \varphi & \dot{\varphi} & \vartheta & \dot{\vartheta} & u_1 & \dot{u}_1 \end{bmatrix}^T$, that contains also the thrust intensity and its derivative. Considering the extended system and the new input, y_1 and y_2 have to be differentiated four and two times, respectively, in order to see the new input $\bar{\mathbf{u}}$ appear:

$$\begin{bmatrix} y_1^{(4)} \\ y_2^{(2)} \end{bmatrix} = \mathbf{b}(\bar{\mathbf{x}}) + \underbrace{\begin{bmatrix} a_2 \cos(x_1+x_3) & -a_2 a_3 \sin(x_1+x_3)u_1 \\ \sin(x_1+x_3) & a_3 \cos(x_1+x_3)u_1 \end{bmatrix}}_{\bar{\mathbf{E}}(\bar{\mathbf{x}})} \bar{\mathbf{u}}, \quad (9)$$

where $\mathbf{b}(\bar{\mathbf{x}})$ is simply derived differentiating equations (7).

The new decoupling matrix $\bar{\mathbf{E}}(\bar{\mathbf{x}})$ is now always invertible except for the zero measure case $u_1 \neq 0$,[3] indeed $\det(\bar{\mathbf{E}}(\bar{\mathbf{x}})) = a_2 a_3 u_1$. Furthermore the total relative degree[4] $r = r_1 + r_2 = 4 + 2 = 6$ is equal to the dimension of the extended state. Therefore the system does not have an internal dynamics [7]. Thus designing the control input as

$$\bar{\mathbf{u}} = \mathbf{E}^{-1}(\bar{\mathbf{x}}) \left[-\mathbf{b}(\bar{\mathbf{x}}) + \mathbf{v} \right], \quad (10)$$

where $\mathbf{v} = [v_1 \ v_2]^T$ are virtual inputs, we obtain $y_1^{(4)} = v_1$ and $y_2^{(2)} = v_2$ i.e., a linear decoupled model equivalent to the original nonlinear system through the state feedback transformation (10).

Given any desired trajectory $y_1^d(t)$ of class C^3 for the link elevation y_1 and any desired trajectory $y_2^d(t)$ of class C^1 for the link stress y_2, one can set the virtual inputs as

$$v_1 = y_1^{d(4)} + k_{11}e_1 + k_{12}e_1^{(1)} + k_{13}e_1^{(2)} + k_{14}e_1^{(3)} \quad (11a)$$

$$v_2 = y_2^{d(2)} + k_{21}e_2 + k_{22}e_2^{(1)}, \quad (11b)$$

where $e_1 = y_1^d - y_1$ and $e_2 = y_2^d - y_2$. Choosing the gains $\mathbf{k}_1 = [k_{11} \ k_{12} \ k_{13} \ k_{14}] \in \mathbb{R}_{>0}^4$ and $\mathbf{k}_2 = [k_{21} \ k_{22}] \in \mathbb{R}_{>0}^2$, one can arbitrarily assign the poles of the error dynamics in order to guaranties an arbitrarily fast exponential tracking of $(y_1^d(t), y_2^d(t))$ for $(y_1(t), y_2(t))$.

The block diagram of the controller is depicted in Fig. 2. We summarize the obtained results in the following:

Proposition 1. *Consider the system composed by a link connected to the ground and an aerial vehicle with passive joints, whose dynamic model is described by (6). Consider as outputs the elevation and the stress of the link, $\mathbf{y} = [\varphi \ f_L]^T$. Then the system is fully linearizable via dynamic feedback for every state configuration, iff the thrust intensity $f_R \neq 0$.*

Furthermore, considering as input the second derivative of the thrust and the torque provided by the aerial vehicle, $\bar{\mathbf{u}} = [\ddot{f}_R \ \tau_R]^T$, the control law described by (10) and (11) globally exponentially steers $\mathbf{y}$ along any desired trajectory $\mathbf{y}^d = [\varphi^d \ f_L^d]^T$ with φ^d of class C^3 and f_L^d of class C^1. The behavior of the convergence can be arbitrarily assigned by suitably choosing $\mathbf{k}_1 \in \mathbb{R}_{>0}^4$, and $\mathbf{k}_2 \in \mathbb{R}_{>0}^2$.

---

[3]In practice, if a trajectory requires zero thrust for a short time, one can switch off the controller when $|u_1| < \varepsilon$ for a sufficiently small $\varepsilon \in \mathbb{R}$.

[4]The sum, for each entry of the output, of the number of times that each output entry has to be differentiated in order to see the input appear.
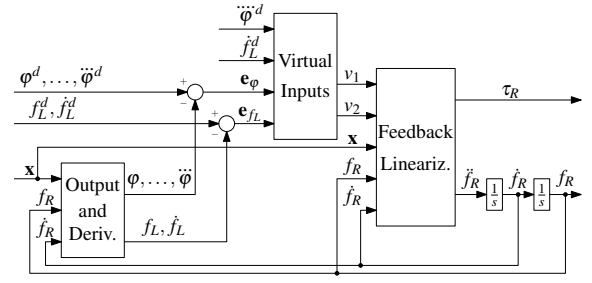

Fig. 2: Graphic representation of the controller.

Remark III.1. Thanks to the exactness of the feedback linearization (i.e., the absence of the internal dynamics) the dynamics of the pitch of the aerial vehicle is automatically stabilized while tracking the desired output.

Remark III.2. If the link is a bar it is completely feasible to pass from compression to tension, and viceversa.

Remark III.3. In the case that the link is a tie (like, e.g., a cable) a preliminary phase has to bring the link in a taut condition. As shown in [8], using a near hovering controller, is possible to reach the initial position and to provide a sufficient force to make the tie taut. Then the control action (10), (11) can be switched on and used to control the stress in the positive domain.

For the equivalence between dynamic feedback linearizability and differential flatness on an open and dense set of the state space [9], the following proposition is valid, whose detailed proof is omitted for space limitation.

Proposition 2. *Consider the model* (1) (2)*, then, the system is flat with respect the flat outputs: elevation and stress of the link, $\mathbf{y} = (\varphi, f_L)$. In other words the state $(\varphi, \dot{\varphi}, \vartheta, \dot{\vartheta})$ and the inputs (f_R, τ_R) can be written as algebraic function of (φ, f_L) and their time derivatives (up to $\varphi^{(4)}$ and $f_L^{(2)}$).*

IV. STATE OBSERVER

Implementation of the control laws (10), (11) requires the knowledge (measurement) of the state $\bar{\mathbf{x}}$, the output $\mathbf{y}$ and its derivatives (up to the third-order for y_1 and first-order for y_2). Nevertheless, $\mathbf{y}$ and all its needed derivatives can be computed from $\bar{\mathbf{x}}$ and $\bar{\mathbf{u}}$ as done, e.g., in (7), (8) and (9) for some of the derivatives. Furthermore, u_1 and $\dot{u}_1$ are internal states of the controller and therefore they are known. Ultimately the knowledge of $\mathbf{x}$ is sufficient in order to implement the presented controller. In this section we demonstrate how the needed $\mathbf{x}$ can be observed based only on the measurements from the onboard IMU (accelerometer plus gyroscope). Then we prove that the observed state can be used in the controller in place of the real state while preserving the closed-loop system stability.

Assume to have an IMU mounted at O_B and oriented according to $\mathscr{F}_B$. The gyroscope provides the angular velocity along $\mathbf{y}_B$, representable in 2D by the scalar $\omega = \dot{\vartheta}$. The accelerometer gives the specific acceleration in $\mathscr{F}_B$, i.e.,

$$\mathbf{a} = R_W^B(\ddot{\mathbf{p}}_B + g\mathbf{z}_W) = [a_x, \ 0, \ a_z]^T, \quad (12)$$

where $R_W^B \in \mathbb{R}^3$ is the rotation matrix from $\mathscr{F}_W$ to $\mathscr{F}_B$. Putting (1) and (3) in (12), we obtain:

$$a_x = \cos(\varphi + \vartheta)\left[l\dot{\varphi}^2 - g\sin\varphi + \frac{f_R}{m}\sin(\varphi + \vartheta)\right] \quad (13\text{a})$$

$$a_z = \sin(\varphi + \vartheta)\left[l\dot{\varphi}^2 - g\sin\varphi + \frac{f_R}{m}\sin(\varphi + \vartheta)\right] - \frac{f_R}{m}. \quad (13\text{b})$$

A. State/Output Transformations and Observability

First of all, since $x_4 = \omega$ is directly measured, we can restrict the observability study and the observer design to the reduced system (6a)–(6c). Then, applying the state transformation $\mathbf{z} = T(\mathbf{x}) : \mathbb{R}^3 \to \mathbb{R}^3$ defined by

$$z_1 = x_1, \qquad z_2 = x_2, \qquad z_3 = x_1 + x_3, \quad (14)$$

and defining the new input $u_3 = x_4 = \omega$, and the new measurements $w_1 = a_x/l$ and $w_1 = a_z/l + f_R/(ml)$, the system (6a)–(6c) is transformed into

$$\begin{cases} \dot{z}_1 = z_2 \\ \dot{z}_2 = a_1 \cos z_1 + a_2 \cos z_3 u_1 \\ \dot{z}_3 = z_2 + u_3 \end{cases} \quad (15)$$

$$\begin{cases} w_1 = \cos z_3 [z_2^2 + a_1 \sin z_1 + a_2 \sin z_3 u_1] \\ w_2 = \sin z_3 [z_2^2 + a_1 \sin z_1 + a_2 \sin z_3 u_1]. \end{cases}$$

Clearly, if we are able to estimate z_1, z_2, z_3 then we can easily recover the original state using $x_1 = z_1, x_2 = z_2, x_3 = z_3 - z_1$.

We then apply another output transformation

$$w_1' = \begin{cases} \frac{w_2}{w_1} = \tan z_3 & \text{if } |\frac{w_2}{w_1}| \le 1 \\ \frac{w_1}{w_2} = \cot z_3 & \text{if } |\frac{w_1}{w_2}| < 1 \end{cases} \quad (16)$$

$$w_2' = \sqrt{w_1^2 + w_2^2} = |z_2^2 + a_1 \sin z_1 + a_2 \sin z_3 u_1|.$$

Note that this transformation is not allowed when $w_2' = 0$. Indeed in this case, both w_1 and w_2 are zero and w_1' cannot be evaluated. From (5), one can notice that $w_2' = |f_L/(ml)|$. Therefore, w_2' is zero when the stress on the link is equal to zero. In the observer design, we shall take into account this singularity, particularly important in the case that the desired stress trajectory passes through zero.

We can now invert the measurement map (16) in order to obtain a direct measure of z_3. However, since the sign of $z_2^2 + a_1 \sin z_1 + a_2 \sin z_3 u_1$ is unknown, one obtains two solutions

$$\bar{w}_1(k) = \begin{cases} \tan^{-1}\left(\frac{w_2}{w_1}\right)_{[-\frac{\pi}{2}, \frac{\pi}{2}]} + k\pi & \text{if } |\frac{w_2}{w_1}| \le 1 \\ \cot^{-1}\left(\frac{w_1}{w_2}\right)_{[0, \pi]} + k\pi & \text{if } |\frac{w_1}{w_2}| < 1 \end{cases}$$

$$\bar{w}_2(k) = \cos(\bar{w}_1(k))w_1 + \sin(\bar{w}_1(k))w_2,$$

where $k \in \{0, 1\}$. Depending on k we have then two distinct pairs of measures: $(\bar{w}_1(0), \bar{w}_2(0))$ and $(\bar{w}_1(1), \bar{w}_2(1))$. We know that, at each time t one of the two pairs of measurements is *correct*, i.e., it is equal to $(z_3, \frac{f_L}{ml})$, while the second one is *wrong*, i.e., it is equal to $(z_3 + \pi, -\frac{f_L}{ml})$. As a matter of fact, it is not possible to discriminate whether the correct one corresponds to $k = 0$ or to $k = 1$ by only considering a single measurement. For the analysis of the

(a) *Global observer.*

(b) *Observer Σ_k:* The first block is the high gain observer, the next is the linear observer for z_1, the third is the state transformation and in the end the prediction error dynamics.
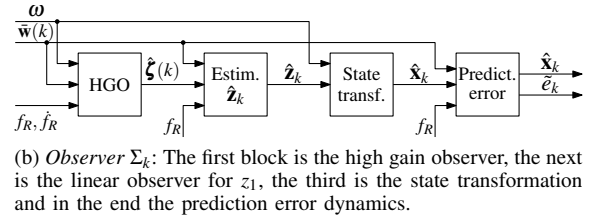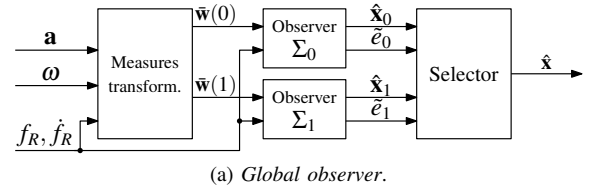
Fig. 3: Graphic representation of the observer.

observability and design of the observer, we consider from now on the correct measurement case. We shall show in Sec. IV-E a discrimination method that exploits the filtering error dynamics. We can then write

$$\bar{w}_1 = z_3, \qquad \bar{w}_2 = z_2^2 + a_1 \sin z_1 + a_2 \sin z_3 u_1 = \frac{f_L}{ml}. \quad (17)$$

In a compact form we can write (15), (17) as

$$\dot{\mathbf{z}} = \mathbf{f}(\mathbf{z}, \mathbf{u}), \qquad \bar{\mathbf{w}} = \mathbf{h}(\mathbf{z}, \mathbf{u}),$$

where $\mathbf{z} = [z_1 \ z_2 \ z_3]^T$, $\mathbf{u} = [u_1 \ u_3]^T$ and $\bar{\mathbf{w}} = [\bar{w}_1 \ \bar{w}_2]^T$. The system is observable if the nonlinear observability matrix $\mathscr{O}(\mathbf{z}, \mathbf{u})$ has full rank [10]. After some algebra (not reported for reason of space) it is possible to see that two minors of $\mathscr{O}(\mathbf{z}, \mathbf{u})$ are equal to $a_1 \cos z_1$ and $a_1 \sin z_1$, respectively, which are never contemporarily zero. Therefore we can conclude that $\mathscr{O}(\mathbf{z}, \mathbf{u})$ is full rank for every $\mathbf{z} \in \mathbb{R}^3$ and $\mathbf{u} \in \mathbb{R}^3$, i.e.:

Proposition 3. *The full state of the system (6) is observable with accelerometer and gyroscope measurements only, except along the trajectories that keep the link stress constantly zero.*

We divide the observer in two parts, as depicted in the block diagram of Fig. 3. The first part makes use of a High Gain Observer (HGO) approach [7], in order to estimate the quantities z_3, z_2, $\dot{z}_2$. The second part applies a nonlinear transformation in order to retrieve z_1. We describe these two parts separately in the next sections.

B. High Gain Observer for z_2 and z_3

Let us define $\zeta_1 = z_3$, $\zeta_2 = z_2$, $\zeta_3 = \dot{z}_2$ and $\boldsymbol{\zeta} = [\zeta_1 \ \zeta_2 \ \zeta_3]^T$ and $\boldsymbol{\mu} = (u_1, \dot{u}_1, u_3)$. Taking the derivative of $\dot{z}_2$ in (15) we can hide the dependency on z_1, in fact:

$$\ddot{z}_2 = -[a_1 \sin z_1 + a_2 \sin z_3 u_1]z_2 - a_2 \sin z_3 u_3 u_1 + a_2 \cos z_3 \dot{u}_1$$
$$= \underbrace{[z_2^2 - \bar{w}_2]z_2 - a_2 \sin z_3 u_3 u_1 + a_2 \cos z_3 \dot{u}_1}_{\sigma(\boldsymbol{\zeta}, \bar{w}_2, \boldsymbol{\mu})}.$$

Therefore, we, can write the dynamics of $\boldsymbol{\zeta}$ as

$$\dot{\boldsymbol{\zeta}} = \underbrace{\begin{bmatrix} 0 & 1 & 0 \\ 0 & 0 & 1 \\ 0 & 0 & 0 \end{bmatrix}}_{\mathbf{A}} \boldsymbol{\zeta} + \underbrace{\begin{bmatrix} u_3 \\ 0 \\ \sigma(\boldsymbol{\zeta}, \bar{w}_2, \boldsymbol{\mu}) \end{bmatrix}}_{\boldsymbol{\sigma}(\boldsymbol{\zeta}, \bar{w}_2, \boldsymbol{\mu})}, \qquad \bar{w}_1 = \underbrace{[1 \ 0 \ 0]}_{\mathbf{C}} \boldsymbol{\zeta}. \quad (18)$$

Thanks to the previous transformations we have been able to put the system in the triangular form (18) for which is possible to use the following high gain observer

$$\dot{\hat{\boldsymbol{\zeta}}} = \mathbf{A}\hat{\boldsymbol{\zeta}} + \boldsymbol{\sigma}(\hat{\boldsymbol{\zeta}}, \bar{w}_2, \boldsymbol{\mu}) + \mathbf{H}(\bar{w}_1 - \mathbf{C}\hat{\boldsymbol{\zeta}}), \quad (19)$$

where $\mathbf{H} = \left[\frac{\alpha_1}{\varepsilon} \; \frac{\alpha_2}{\varepsilon^2} \; \frac{\alpha_3}{\varepsilon^3}\right]^T$, $\varepsilon \in \mathbb{R}_{>0}$, and $\alpha_i \in \mathbb{R}_{>0}$ are set such that the roots of $s^3 + \alpha_1 s^2 + \alpha_2 s + \alpha_3$ have negative real part.[5]

C. Observation of z_1 and Final $\hat{\mathbf{x}}$

From the expressions of $\dot{z}_2$ in (15) and $\bar{w}_2$ in (17) we have:

$$\begin{bmatrix} \cos z_1 \\ \sin z_1 \end{bmatrix} = \frac{1}{a_1} \begin{bmatrix} \dot{z}_2 - a_2 \cos z_3 u_1 \\ \bar{w}_2 - z_2^2 - a_2 \sin z_3 u_1 \end{bmatrix} = \mathbf{h}(\boldsymbol{\zeta}, u_1, \bar{w}_2).$$

The state z_1 can then be interpreted as the phase of the unit-vector $\mathbf{h}(\boldsymbol{\zeta}, u_1, \bar{w}_2)$, which we denote with $\angle \mathbf{h}(\boldsymbol{\zeta}, u_1, \bar{w}_2)$. We can then obtain a direct estimate of z_1 as

$$\hat{z}_1 = \angle \mathbf{h}(\hat{\boldsymbol{\zeta}}, u_1, \bar{w}_2). \quad (20)$$

It is easy to see that the convergence of $\hat{\boldsymbol{\zeta}}$ to $\boldsymbol{\zeta}$ automatically implies the convergence of $\hat{z}_1$ to z_1.

Finally, using the first state transformation (14), we get the estimation of the original state $\hat{\mathbf{x}} = (\hat{x}_1, \hat{x}_2, \hat{x}_3, \hat{x}_4)$ needed by the controller shown in Sec. III, i.e,:

$$\hat{x}_1 = \hat{z}_1, \quad \hat{x}_2 = \hat{z}_2, \quad \hat{x}_3 = \hat{z}_3 - \hat{z}_1, \quad \hat{x}_4 = u_3. \quad (21)$$

D. Closed-loop System Stability with State Observation

Due to space limitations we provide here only the main steps of the convergence proof for the controlled closed loop system with observer. From (20) and (21) we can notice that the estimated state, $\hat{\mathbf{x}}$, is a function of $\hat{\boldsymbol{\zeta}}$, $\bar{w}_2$ and u_3

$$\hat{\mathbf{x}} = T(\hat{\boldsymbol{\zeta}}, \bar{w}_2, u_3). \quad (22)$$

Therefore, writing the output controller (10) as function of the estimated state, and replacing (22) we obtain

$$\bar{\mathbf{u}} = \Gamma(\hat{\mathbf{x}}, u_1, \dot{u}_1) = \bar{\Gamma}(\hat{\boldsymbol{\zeta}}, \bar{w}_2, u_3, u_1, \dot{u}_1).$$

The controller depends only on the estimation of the HGO, the measures, and the states of the dynamic compensator. Then, since the system is observable, it can be transformed in triangular form, and the controller stabilizes the nominal system, there exists $\varepsilon^* > 0$ such that, for every $0 < \varepsilon < \varepsilon^*$, the error dynamic of the observer and the closed-loop system are asymptotically stable [7].

The observer presented here is globally convergent. However, to minimize the transient phase it is wise to use some method to initialize the estimate as close as possible to the actual state. For example one can use for this purpose the method proposed in [5], which produces an acceptable estimate for quasi-static motions and a distorted estimate for more general motions.

---

[5] The difference $(\bar{w}_1 - \mathbf{C}\hat{\boldsymbol{\zeta}})$ stands here for the unique angle $\beta \in (-\pi, \pi]$ such that $\beta + \mathbf{C}\hat{\boldsymbol{\zeta}} = \bar{w}_1 + k2\pi$ for a certain $k \in \mathbb{Z}$.

E. Disambiguation of $\bar{\mathbf{w}}$

Using the gyroscope measure, $u_3 = \omega$, and the knowledge of the control inputs, the observer Σ_k, described by (19) (20) (21), based on the measures $\bar{\mathbf{w}}(k)$, provides an estimation of the state $\hat{\mathbf{x}}_k = (\hat{x}_{1k}, \hat{x}_{2k}, \hat{x}_{3k}, \hat{x}_{4k})$, depending on $k = \{0, 1\}$. Implementing this observer for both the k values, we get two estimations of the same state, $\hat{\mathbf{x}}_0$ and $\hat{\mathbf{x}}_1$. Thus the problem arises of which observer should be considered as the correct one. We propose here a selection method based on the prediction error. We assign to each observer a prediction error $\tilde{e}_k$, smoothed with an exponential discount factor:

$$\dot{\tilde{e}}_k = \lambda \left(\|\mathbf{w} - \hat{\mathbf{w}}_k\| - \tilde{e}_k \right), \quad (23)$$

where $\lambda \in \mathbb{R}_{>0}$ sets the discount rate, $\mathbf{w} = [w_1 \; w_2]^T = \left[\frac{a_x}{l} \; \frac{a_x}{l} + \frac{f_R}{ml} \right]^T$, and $\hat{\mathbf{w}}_k = [\hat{w}_{1k} \; \hat{w}_{2k}]^T$ is defined as

$$\begin{aligned} \hat{w}_{1k} &= \cos(\hat{x}_{1k} + \hat{x}_{3k}) [\hat{x}_{2k}^2 + a_1 \sin \hat{x}_{1k} + a_2 \sin(\hat{x}_{1k} + \hat{x}_{3k}) u_1] \\ \hat{w}_{2k} &= \sin(\hat{x}_{1k} + \hat{x}_{3k}) [\hat{x}_{2k}^2 + a_1 \sin \hat{x}_{1k} + a_2 \sin(\hat{x}_{1k} + \hat{x}_{3k}) u_1]. \end{aligned} \quad (24)$$

Then we select the estimation provided by the observer with the minimum prediction error

$$\hat{\mathbf{x}} = \begin{cases} \hat{\mathbf{x}}_0 & \text{if } \tilde{e}_0 \leq \tilde{e}_1 \\ \hat{\mathbf{x}}_1 & \text{if } \tilde{e}_1 < \tilde{e}_0. \end{cases}$$

If the system starts with zero elevation rate (i.e., $x_2 = 0$), after a transient the two estimations will converge to

$$\hat{x}_{1k} = x_1 + k\pi \quad \hat{x}_{2k} = 0 \quad \hat{x}_{3k} = x_3 \quad \hat{x}_{4k} = x_4,$$

where (x_1, x_2, x_3, x_4) are the real state. In this condition, from equation (24) it is easy to verify that the prediction errors of the two observers converge both to zero. Thus the proposed method could select the incorrect observer. Nevertheless, this is not a problem in practice. Because, by computing the control action based on the wrong estimation, the controller will react forcing $x_2 \neq 0$ and, in turn, the predictions errors to be different from each other.

V. SIMULATIONS

We conducted several simulations using Simulink and modeling the system with the toolbox *SimMechanics*, thus obtaining a more realistic validation independently from the model used for the control and observer design. In all the simulations we consider an aerial robot of mass $m_R = 1\,[\text{Kg}]$ and moment of inertia $J_R = 0.15\,[\text{Kg}\,\text{m}^2]$, connected to the ground with a generic link of length $l = 2\,[\text{m}]$. We assume the vehicle is able to provide both positive and negative thrust. The gains $\mathbf{k}_1$ and $\mathbf{k}_2$ in (11) are chosen such that the poles of the error dynamics e_1 and e_2 are placed in $(-3, -6, -12, -24)$ and in $(-6, -12)$ respectively. We set $\varepsilon = 0.1$ and $(\alpha_1, \alpha_2, \alpha_3)$ in (19) in order to obtain an error dynamics with negative real poles. The discount rate in (23) is set to $\lambda = 20$.

Each simulation considers different initial state and pair of desired trajectories for the stress and elevation. The complete set of simulation results is provided in [11]. We show in Fig. 4 a representative simulation chosen from that set. Each simulation result is composed by three figures showing: a stroboscopic trajectory, the controller plots and the observer plots, respectively.

In the stroboscopic trajectories (as the one in Fig 4a) we show the trajectory evolution as a sequence of state images discriminated by the color that represents the time. In order to show the stress variation, the width of the link is thinner when the tension is higher, and wider when the compression is higher. Moreover to better distinguish the positive from the negative stresses, we draw the link dashed or solid, respectively. This recalls the usual mechanical behavior of a bar under stress. Similarly, the arrow representing the thrust vector is wider and longer when the thrust intensity is higher.

In the controller and observer plot figures (like the ones in Figs. 4b, and 4c) it is possible to see that, after a transient due to the state estimation convergence, the controller is able to obtain an exact tracking of all the desired trajectories for both the elevation and stress of the link. This is also obtained for desired stress trajectories passing from tension to compression and viceversa. One can also notice that the transition from tension to compression is also stable and that compression is automatically achieved with a facing down attitude and positive thrust.

A video of the simulations is available in the supplementary material. Additional simulations are provided in [11].

VI. CONCLUSIONS

We presented a solution to a new tethered aerial vehicle problem that goes beyond the quasi static case considered in the literature. We showed the possibility to precisely and independently control tension and compression of a generic link only resorting to onboard inertial measurements.

In the future we plan to experimentally validate the proposed approach and to design a trajectory planner based on the proven differential flatness of the tethered vehicle.

REFERENCES

[1] I. Maza, K. Kondak, M. Bernard, and A. Ollero, "Multi-UAV cooperation and control for load transportation and deployment," *Journal of Intelligent & Robotics Systems*, vol. 57, no. 1-4, pp. 417–449, 2010.
[2] M. F. Pinkney, D. Hampel, and S. DiPierro, "Unmanned aerial vehicle (UAV) communications relay," in *Military Communications Conference, 1996*, vol. 1, Oct. 1996, pp. 47–51.
[3] F. Muttin, "Umbilical deployment modeling for tethered UAV detecting oil pollution from ship," *Applied Ocean Research*, vol. 33, no. 4, pp. 332–343, 2011.
[4] L. A. Sandino, M. Bejar, K. Kondak, and A. Ollero, "Advances in modeling and control of tethered unmanned helicopters to enhance hovering performance," *Journal of Intelligent & Robotics Systems*, vol. 73, no. 1-4, pp. 3–18, 2014.
[5] S. Lupashin and R. D'Andrea, "Stabilization of a flying vehicle on a taut tether using inertial sensing," in *2013 IEEE/RSJ Int. Conf. on Intelligent Robots and Systems*, Tokyo, Japan, Nov 2013, pp. 2432–2438.
[6] M. M. Nicotra, R. Naldi, and E. Garone, "Taut cable control of a tethered UAV," in *19th IFAC World Congress*, Cape Town, South Africa, Aug. 2014, pp. 3190–3195.
[7] H. K. Khalil, *Nonlinear Systems*, 3rd ed. Prentice Hall, 2001.
[8] G. Gioioso, M. Ryll, D. Prattichizzo, H. H. Bülthoff, and A. Franchi, "Turning a near-hovering controlled quadrotor into a 3D force effector," in *2014 IEEE Int. Conf. on Robotics and Automation*, Hong Kong, China, May. 2014, pp. 6278–6284.
[9] A. De Luca and G. Oriolo, "Trajectory planning and control for planar robots with passive last joint," *The International Journal of Robotics Research*, vol. 21, no. 5-6, pp. 575–590, 2002.
[10] R. Marino and P. Tomei, *Nonlinear Control Design: Geometric, Adaptive and Robust*. Prentice Hall, 1996.
[11] M. Tognon and A. Franchi, "Extended simulations for the link stress and elevation control of a tethered aerial robot," LAAS-CNRS, Tech. Rep. hal-01118868, Feb. 2015.
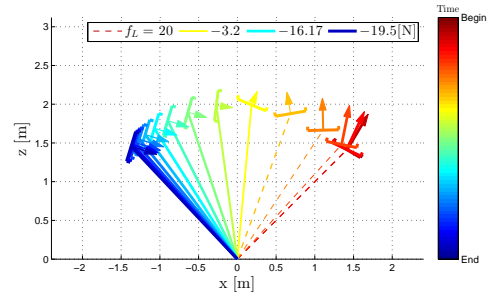
(a) Trajectory from time Begin $= 2\,[\mathrm{s}]$ to End $= 4.5\,[\mathrm{s}]$.
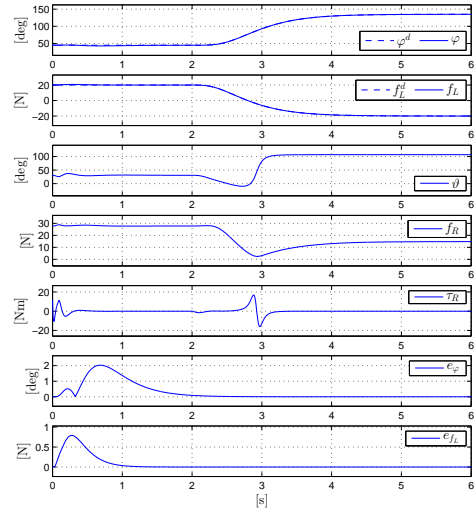
(b) Controller Results: thrust stays positive even when the strees becomes negative and compression is obtained turning the robot.
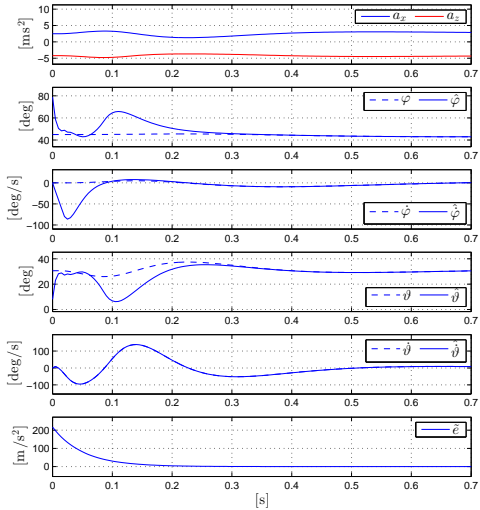
(c) Observer Results: zoom on the first 0.7 seconds of simulation. The remaining part is not displayed because the observer follows the state with high fidelity. $\dot{\vartheta}$ and $\hat{\dot{\vartheta}}$ are always equal because the estimated value comes from the direct measure of the gyroscope. The prediction error does not increase even when the tension goes to zero for an instant.

Fig. 4: The desired smooth elevation trajectory of class C^3 goes from the initial value $\varphi_0^d = \pi/4\,[\mathrm{rad}]$ to the final $\varphi_f^d = 3\pi/4\,[\mathrm{rad}]$. The desired smooth stress trajectory of class C^1 goes from the initial tension $f_{L\,0}^d = 20\,[\mathrm{N}]$ to the final compression $f_{L\,f}^d = -20\,[\mathrm{N}]$. The complete simulation results can be found in [11].